BIOLOGY OF REPRODUCTION (2016) **94**(6):125, 1–12
Published online before print 27 April 2016.
DOI 10.1095/biolreprod.115.137687

# Growing Mouse Oocytes Transiently Activate Folate Transport via Folate Receptors As They Approach Full Size[1]

**Megan Meredith,[3,4] Allison H. MacNeil,[3] Jacquetta M. Trasler,[5,6] and Jay M. Baltz[2,3,4]**

[3]*Ottawa Hospital Research Institute, Ottawa, Ontario, Canada*
[4]*Department of Obstetrics and Gynecology and Department of Cellular and Molecular Medicine, University of Ottawa Faculty of Medicine, Ottawa, Ontario, Canada*
[5]*Montréal Children's Hospital and Research Institute of the McGill University Health Centre, Montréal, Quebec, Canada*
[6]*Departments of Human Genetics, Pediatrics, and Pharmacology and Therapeutics, McGill University, Montréal, Quebec, Canada*

## ABSTRACT

**The folate cycle is central to cellular one-carbon metabolism, where folates are carriers of one-carbon units that are critical for synthesis of purines, thymidylate, and S-adenosylmethionine, the universal methyl donor that forms the cellular methyl pool. Although folates are well-known to be important for early embryo and fetal development, their role in oogenesis has not been clearly established. Here, folate transport proteins were detected in developing neonatal ovaries and growing oocytes by immunohistochemistry, Western blot, and immunofluorescence. The folate receptors FOLR1 and FOLR2 as well as reduced folate carrier 1 (RFC1, SLC19A1 protein) each appeared to be present in follicular cells including granulosa cells. In growing oocytes, however, only FOLR2 immunoreactivity appeared abundant. Localization of apparent FOLR2 immunofluorescence near the plasma membrane increased with oocyte growth and peaked in oocytes as they neared full size. We assessed folate transport using the model folate leucovorin (folinic acid). Unexpectedly, there was a transient burst of folate transport activity for a brief period during oocyte growth as they neared full size, while folate transport was otherwise undetectable for the rest of oogenesis and in fully grown germinal vesicle stage oocytes. This folate transport was inhibited by dynasore, an inhibitor of endocytosis, but insensitive to the anion transport inhibitor stilbene 4-acetamido-40-isothiocyanato-stilbene-2,20-disulfonic acid, consistent with folate receptor-mediated transport but not with RFC1-mediated transport. Thus, near the end of their growth, growing oocytes may take up folates that could support the final stage of oogenesis or be stored to provide the endogenous folates needed in early embryogenesis.**

*folates, follicular development, metabolism, oocyte development, transport*

## INTRODUCTION

The folate cycle is a central component of one-carbon (1C) metabolism in mammalian cells, acting as the shuttle for 1C units that are transferred onto a range of substrates [1, 2]. The products of the folate cycle include thymidylate, purines, the cellular methyl pool, and polyamines [3, 4]. The folate cycle is directly connected to purine and thymidylate synthesis [1, 5], while its function in the synthesis of the cellular methyl pool and polyamines is through its role in supplying 1C units to the methionine cycle that produces S-adenosylmethionine (SAM). SAM is formed by remethylation of homocysteine to produce methionine that is then reacted with adenosine to yield SAM [3, 6]. In virtually all cells, methyl groups transferred from serine to produce 5-methyltetrahydrofolate are the principle source of the methyl groups used in homocysteine remethylation [5, 6]. SAM, in turn, serves as the substrate that donates methyl groups to a large array of cellular methyltransferases [3, 6, 7] or is metabolized for polyamine synthesis [6].

Disruptions in folate metabolism or an inadequate supply of folates are particularly problematic during early development, causing a characteristic set of problems in postimplantation embryos and fetuses that notably include neural tube defects [8]. The role of folates in the embryo before its implantation in the uterus has not been nearly as well studied as in postimplantation embryonic and fetal development [9, 10]. It has, however, been found that preimplantation embryos require folates for thymidylate and purine synthesis because inhibiting folate metabolism with the antifolate methotrexate arrests embryo development, which can then be rescued with exogenously supplied thymidine and hypoxanthine [11–13]. In the mouse, methotrexate in the absence of thymidine and hypoxanthine prevented cleavage to the next stage at each stage assessed starting at the 1-cell stage [11]. A role in methyl pool synthesis in preimplantation embryos is also indicated because blocking folate metabolism results in decreased SAM in the mouse blastocyst [13].

Methylation of DNA on cytosines is a key epigenetic mechanism in mammals that is mediated by DNA methyltransferases using SAM as the methyl donor [14]. Generally, each tissue has a characteristic pattern of DNA methylation that is maintained through cell divisions. However, global DNA methylation is almost entirely erased twice during the life cycle. The first erasure occurs in primordial germ cells, after which gamete-specific methylomes are established during oocyte growth and spermatogenesis [15, 16]. The second is during early preimplantation embryogenesis, after which the embryonic methylome is initially established during the peri-

[1]Funded by the Canadian Institutes of Health Research operating grant MOP97972.
[2]Correspondence: Jay M. Baltz, Ottawa Hospital Research Institute, 501 Smyth Rd., Mailbox 411, Ottawa, ON K1H8L6, Canada.
E-mail: jbaltz@ohri.ca

Received: 9 December 2015.
First decision: 14 January 2016.
Accepted: 19 April 2016.

eISSN: 1529-7268 http://www.biolreprod.org
ISSN: 0006-3363

implantation period [13, 17, 18]. Thus, there is likely a need for methyl pools during oocyte growth and again in the peri-implantation embryo. In the peri-implantation blastocyst, it was shown that disrupting folate metabolism, in conjunction with blocking an alternative pathway for methyl generation in preimplantation embryos that uses betaine (N,N,N-timethylglycine) as the methyl donor [19], prevents the increase in DNA methylation that begins in the inner cell mass [13].

Although intracellular folates are recycled after donating 1C units in the folate cycle, cells nevertheless must initially accumulate folates and then continually replenish those that are lost from cells or degraded. Folates are derived from the diet because they cannot be synthesized by mammalian cells. The initial absorption of folates is via a specialized intestinal transporter, the proton-coupled folate transporter (PCFT), encoded by the *Slc46a1* gene [20], after which circulating folates are taken up by cells throughout the body.

In most somatic cells, the primary mechanism for transporting folates from the extracellular fluid is the reduced folate carrier, RFC1, whose molecular identity is the SLC19A1 protein [21–23]. Another mechanism for cellular folate transport is via folate receptors, of which there are two isoforms in mice, FOLR1 (also known as FR$\alpha$) and FOLR2 (FR$\beta$) [23, 24]. RFC1 and the folate receptors function by distinct mechanisms. RFC1 (SLC19A1) is an antiporter that exchanges folate for inorganic phosphate [23, 25, 26] while the folate receptors bind folates and are then endocytosed [25, 27, 28].

Because preimplantation embryos do not have a strict requirement for exogenous folates in vitro, it was originally proposed that they utilized only endogenous folates that the egg or oocyte had accumulated before fertilization [11]. More recently it was found that mouse embryos from the 2-cell through blastocyst stages also take up folates from their external environment via active FOLR1-mediated endocytosis [25], possibly to better meet an increased need for folate during the peri-implantation period. Nevertheless, it is clear that preimplantation embryo development can be adequately supported by endogenous folates because many successful embryo culture media contain no folates. The origin of these endogenous folates accumulated prior to the 2-cell stage is, however, unknown. Similarly, it is not known whether oocytes accumulate folates during oogenesis, particularly during the establishment of the oocyte methylome.

Previously, we showed that the cumulus granulosa cells surrounding fully grown germinal vesicle (GV) stage mouse oocytes take up folates via RFC1 [25]. However, despite the presence of functional gap junctions connecting the cumulus cells to the enclosed oocyte, no transfer of folate from the cumulus to the oocyte was detected, nor did fully grown oocytes themselves take up folates at a detectable level [25]. Therefore, to determine the source of folates in oocytes and early preimplantation embryos, we have investigated whether growing oocytes actively take up folates during oogenesis.

## MATERIALS AND METHODS

### Chemicals and Media

All the chemicals were obtained from Sigma-Aldrich Canada Ltd. unless otherwise specified. Modified KSOM [29] embryo culture medium was used with oocytes and follicles, and oocyte collection was done in modified HEPES-KSOM as previously described [25]. KSOM was equilibrated with 5% $CO_2$ in air, and HEPES-KSOM was adjusted to pH 7.4.

### Oocyte, Follicle, Embryo, and Tissue Collection

All the animal protocols were approved by the Animal Care Committee of the University of Ottawa. Growing oocytes and follicles were obtained from postnatal female CF1 mice (Crl:CF1; Charles River) on Postnatal Days 5–21 (P5–21) after birth exactly as previously described [30]. During this period, a large cohort of follicles undergoes a coordinated wave of growth so that relatively homogeneous populations of synchronously growing oocytes and follicles can be obtained on each day, ranging from small oocytes in primary follicles on P5 to fully grown oocytes in antral follicles on P21 [30, 31]. Ovaries were removed from postnatal females, and the follicles were isolated enzymatically with collagenase (before P15) or mechanically by mincing (P15 and later) as previously described [30]. Where specified, the diameters of the oocytes were measured using an eyepiece reticle on an inverted microscope (Zeiss Axiovert S100) and the oocytes sorted into groups in 5 μm increments.

Fully grown GV stage oocytes, cumulus-oocyte complexes (COCs), and preimplantation embryos were obtained as previously described [10, 25, 32] from female CF1 mice (4–6 wk old; Charles River) that had been superovulated by intraperitoneal injection of 5 IU equine chorionic gonadotropin (eCG) (Merck Folligon; Intervet). COCs were collected at 44–46 h post-eCG and either used intact or the enclosed GV oocyte isolated by repeated pipetting through a narrow-bore pipette. For embryos, females were injected intraperitoneally with 5 IU human chorionic gonadotropin (hCG) (Merck Chorulon, Intervet) 47.5 h post-eCG, and caged overnight with BDF1 (B6D2F1/Crl) males (Charles River). Two-cell embryos were removed from oviducts at ~44 h and blastocysts from uteri at ~94 h post-eCG. All the collections were performed in HEPES-KSOM.

Ovaries for immunohistochemistry were collected from neonatal CF1 females on P5, P11, P15, and P21 and from Embryonic Day 17 (E17) fetuses as described below. Placenta lysates used in Western blots were normal mouse placenta whole cell lysate (ab29139; Abcam).

### Primary Antibodies

The same primary antibodies were used for immunocytochemistry on ovary sections, Western blots, and immunofluorescence. Primary antibodies were chosen based on initial Western blot screens (not shown) with positive control tissues or overexpression lysates to identify those with a strong band near the expected position and the fewest nonspecific bands. FOLR1 was detected with Abcam ab67422 (polyclonal rabbit immunoglobulin G [IgG], affinity purified). FOLR2 was detected with GeneTex (Irvine, CA) GTX105822 (polyclonal rabbit IgG, affinity purified). RFC1 (SLC19A1) was detected with Abcam ab62302 (polyclonal rabbit IgG, protein A purified). Each was supplied as 1 mg/ml. For Western blot loading controls, β-tubulin was detected with ab6046 and β-actin with ab8227 (both rabbit IgG; Abcam).

### Immunohistochemistry

Ovaries were obtained from postnatal (P5, P11, P15, P21) or embryonic (E17) female CF1 mice and fixed overnight at 4°C with 4% paraformaldehyde in phosphate-buffered saline (PBS) and then washed three times in PBS (5 min each). The ovaries were then stained with Nuclear Fast Red (N3020) to allow visualization during embedding, washed three times in water, and stored in 70% ethanol until embedding. Ovaries were embedded in agarose and cut into 5 μm sections that were mounted on slides and heated to 110°C in citrate buffer (pH 6.0) for 12 min for epitope retrieval. Embedding, sectioning, and immunohistochemistry were performed by the PALM Histology Core Facility, University of Ottawa Faculty of Medicine.

All antibodies used were first optimized using positive control mouse tissues processed identically to the ovaries (data not shown). Ovary sections were incubated with primary antibodies for 1 h at room temperature at the following dilutions: 1:100 SLC19A1 (RTC1), 1:250 FOLR1, and 1:250 FOLR2 (GTX). The MACH4 alkaline phosphatase anti-rabbit detection system (Biocare Medical) was used according to the manufacturer's instructions. Sections from each ovary were stained with hematoxylin/eosin (H&E) for visualization.

### Western Blots

Oocytes, embryos, COCs, or tissues were solubilized in modified RIPA buffer (20 mM Tris-HCl pH 7.4, 150 mM NaCl, 1 mM ethylenediaminetetraacetic acid, 1% Triton X-100, 1% sodium deoxycholate, 0.1% SDS, 1 mM phenylmethylsulfonyl fluoride, 5 μg/ml aprotinin, 5 μg/ml leupeptin). Oocytes, embryos, or COCs were obtained from several females in one collection procedure and pooled to give the number specified as being loaded per lane (generally 50 or 100), and each pooled set was considered one independent

repeat. Proteins were separated on 12% SDS-PAGE gels, transferred to nitrocellulose membranes, and the membranes incubated with primary antibodies in blocking solution overnight at 4°C. Proteins were detected using the following primary antibody dilutions and blocking solutions: 1:1000 FOLR1 in 2% BSA, 1:1000 FOLR2 in 5% milk powder, 1:500 RFC1 (SLC19A1) in 1% BSA, and 1:500 β-tubulin or β-actin in 5% milk powder. These conditions had been optimized for folate transporters using positive control lysates (not shown). For all primary antibodies, the secondary antibody was 1:5000 goat anti-rabbit horseradish peroxidase-conjugated IgG (1706515; Bio-Rad Laboratories). Chemiluminescent detection was with the Amersham ECL Prime kit (RPN2232; GE Healthcare) except for β-tubulin and β-actin where the Thermo Scientific Pierce ECL kit (32209; ThermoFisher Scientific) was used.

Although the best-performing antibodies available were chosen based on preliminary screens, nonspecific bands were also present. The FOLR1 antibody used (ab67422; Abcam) showed strong reactivity at the expected position (an apparent doublet or triplet at ~32 kDa) and no other strong bands, although on some blots, there were weak bands at ~40 and ~70 kDa. The FOLR2 antibody (GTX105822; GeneTex) showed a strong band near the expected position (~27–31 kDa, see below) but also had a single additional, apparently nonspecific band near 75 kDa. The SLC19A1 antibody (ab62302; Abcam) yielded a strong band near the expected position (~62 kDa) but also had bands at ~40 and ~80 kDa.

Where specified, deglycosylation was performed with the endoglycosidase peptide-N-glycosidase F (PNGase F) (P0704S; New England Biolabs) according to the manufacturer's protocol with denaturing conditions. Briefly, samples were denatured at 95°C for 5 min and then deglycosylated with 500 U PNGase F for 10 min at 37°C. Deglycosylation of RNAse B (5 μg, P7817S; New England Biolabs) and of human FOLR2 overexpressed in HEK293T cells (LY400280; OriGene) was used to confirm the activity. Negative control samples had water rather than PNGase F solution added. The reaction was terminated by adding Laemmi buffer and 5% β-mercaptoethanol and boiling for 5 min.

### Immunofluorescence

P15 oocytes, blastocysts, or COCs were collected, and the zona pellucida removed from oocytes and blastocysts by brief exposure to acid Tyrode solution. Groups of 5–10 oocytes or embryos were processed simultaneously. They were fixed with 2% paraformaldehyde in PBS for 20 min at room temperature. The fixed samples were treated with 0.05% Tween-20 in PBS for at least 48 h at 4°C and then stored in the same solution until used. Before incubating with a primary antibody, the FOLR2 epitope (but not FOLR1 or SLC19A1) required unmasking in 1% SDS in PBS for 2.5 min at room temperature. They were then incubated in blocking solution (5% fetal bovine serum and 0.01% Tween-20 in PBS) for 1 h at 37°C, and then with primary antibody in antibody dilution buffer (ADB) (1% fetal bovine serum and 0.003% Tween-20 in PBS) overnight at 4°C. All the primary antibodies were used at a 1:50 dilution. They were then washed four times in ADB and incubated with Alexa 594 goat anti-rabbit IgG (1:200, A11037; ThermoFisher) for 1 h. After washing three times in ADB, samples were mounted on slides in a well with SlowFade antifade reagent (S2828; ThermoFisher) and imaged using a Zeiss LSM 510 confocal with a 40× oil-immersion objective. Where indicated, samples were costained before mounting with Alexa-488 wheat germ agglutinin (10 μg/ml, W11261; Invitrogen) and Hoechst 33342 (25 μg/ml, B2261) in ADB to allow visualization of the membrane and nuclei.

### Folate Transport Measurements

Folate transport into oocytes and follicles was measured using leucovorin (LV, also known as folinic acid) as a model folate transporter substrate exactly as previously described [25, 33]. $^{3}$H-labeled LV ([$^{3}$H] LV) was obtained as (3′,5′,7,9-$^{3}$H [N])-(6S)-leucovorin, diammonium salt (MT521; Movarek) in 50% ethanol in water with a specific activity of 5–25 Ci (185–925 GBq)/mmol. Unlabeled LV was obtained from Sigma-Aldrich (folinic acid calcium salt, F7878). Oocytes or follicles were incubated for 20 min with 2 μM [$^{3}$H] LV in KSOM drops under oil at 37°C. The instantaneous inward transport rate was calculated by dividing the amount of LV accumulated by the time of incubation. The nonsaturable, nonspecific component of LV transport was determined in the presence of 1 mM unlabeled LV.

Incubation with a low micromolar amount of a radiolabeled compound for a short period of time followed by measurement of the amount of the compound that has been taken up into the cell yields a measure of the rate of inward transport [33–35]. A low concentration is used to minimize any nonspecific component of transport (e.g., transmembrane diffusion), while a short incubation time minimizes the possibility that enough labeled compound accumulates in the cell to allow significant back-flux out of the cell or incorporation into intracellular sinks (e.g., by metabolism). Any nonsaturable, nonspecific transport is revealed by competition with a large excess of unlabeled substrate, which is subtracted so that only saturable transport is measured. Thus, these measurements yield the rate of saturable, transporter-mediated transport into cells [35].

Where indicated, potential inhibitors of folate transport were included in the medium during the 20 min incubation period. To target RFC1 activity, stilbene 4-acetamido-40-isothiocyanato-stilbene-2,20-disulfonic acid (SITS) (1 mM, dissolved directly in KSOM), a broad-specificity anion transport inhibitor that effectively blocks RFC1 activity [25, 36], was used. To target folate receptor activity, dynasore (80 μM, added from a 1000× stock in dimethylsulfoxide), a dynamin GTPase inhibitor that blocks endocytosis, including of folate receptors [25, 37], was used. For dynasore, 0.1% dimethylsulfoxide was used as a vehicle-only control. After washing six times in cold HEPES-KSOM, $^{3}$H content of oocytes or follicles was determined by liquid scintillation counting as previously described [25]. Background was determined from an equal volume of the last wash drop and subtracted from the measured values.

### Data Analysis

Quantitative data were expressed as the mean ± SEM and plotted using Prism 5 (GraphPad). Means were compared by ANOVA with Tukey post hoc test for multiple (>2) comparisons or Student two-tailed *t*-test for comparing two means, using Prism. Where a pool of oocytes or follicles was divided into several treatment groups and handled in parallel within each independent repeat, initial testing (Prism) was performed to determine if the effect of matching in ANOVA or pairing in *t*-tests was significant, in which cases matched ANOVA or paired *t*-tests were used. Differences were assumed to be significant at $P < 0.05$.

Images were cropped where necessary using ImageJ 1.48 (National Institutes of Health) and composites assembled using Photoshop CC 2015 (Adobe). Image manipulations were limited to setting the minimum and maximum brightness levels, which were applied equally to all panels within an image except where noted.

## RESULTS

### Expression of Folate Transporters During Oogenesis

To determine whether folate transporter proteins are expressed in oocytes during oogenesis, we performed immunocytochemistry for SLC19A1 (RFC1), FOLR1, and FOLR2 on sections of embryonic and neonatal ovaries (Fig. 1), which contain relatively homogeneous cohorts of growing oocytes at defined stages of development [38–40]. Some FOLR1 immunostaining was present in somatic cells on E17.5, and then substantial FOLR1 was present in both granulosa and theca cells in growing follicles. FOLR1 appeared to decrease in granulosa cells by P21. Light FOLR1 immunostaining was evident in growing oocytes. FOLR2 immunostaining was very pronounced in oocytes at all stages of growth from P5 and was also present in granulosa cells throughout follicular growth. SLC19A1 was absent during follicular and oocyte growth, but became apparent in granulosa cells in antral follicles (P21). Thus, only FOLR2 immunoreactivity was substantially apparent in oocytes, while the somatic cell compartment appeared to express multiple folate transport proteins.

We then investigated the pattern of folate transporter protein expression in growing (P15) oocytes by Western blots. Consistent with the immunohistochemistry results, there was little or no FOLR1 evident in growing oocytes (Fig. 2A). It was present at a high level in blastocysts, but was absent or at low levels in fully grown GV stage oocytes or 2-cell stage embryos, which is consistent with our previous demonstration of substantial folate receptor activity attributed to FOLR1 in blastocysts, lower activity in 2-cell embryos, and undetectable activity in GV oocytes [25].

SLC19A1 (RFC1) protein was detected in COCs, but not in growing oocytes or blastocysts (Fig. 2B). A lower level of RFC1 was evident in GV oocytes, although this could be due to remnants of cumulus cells within the zona pellucida. This

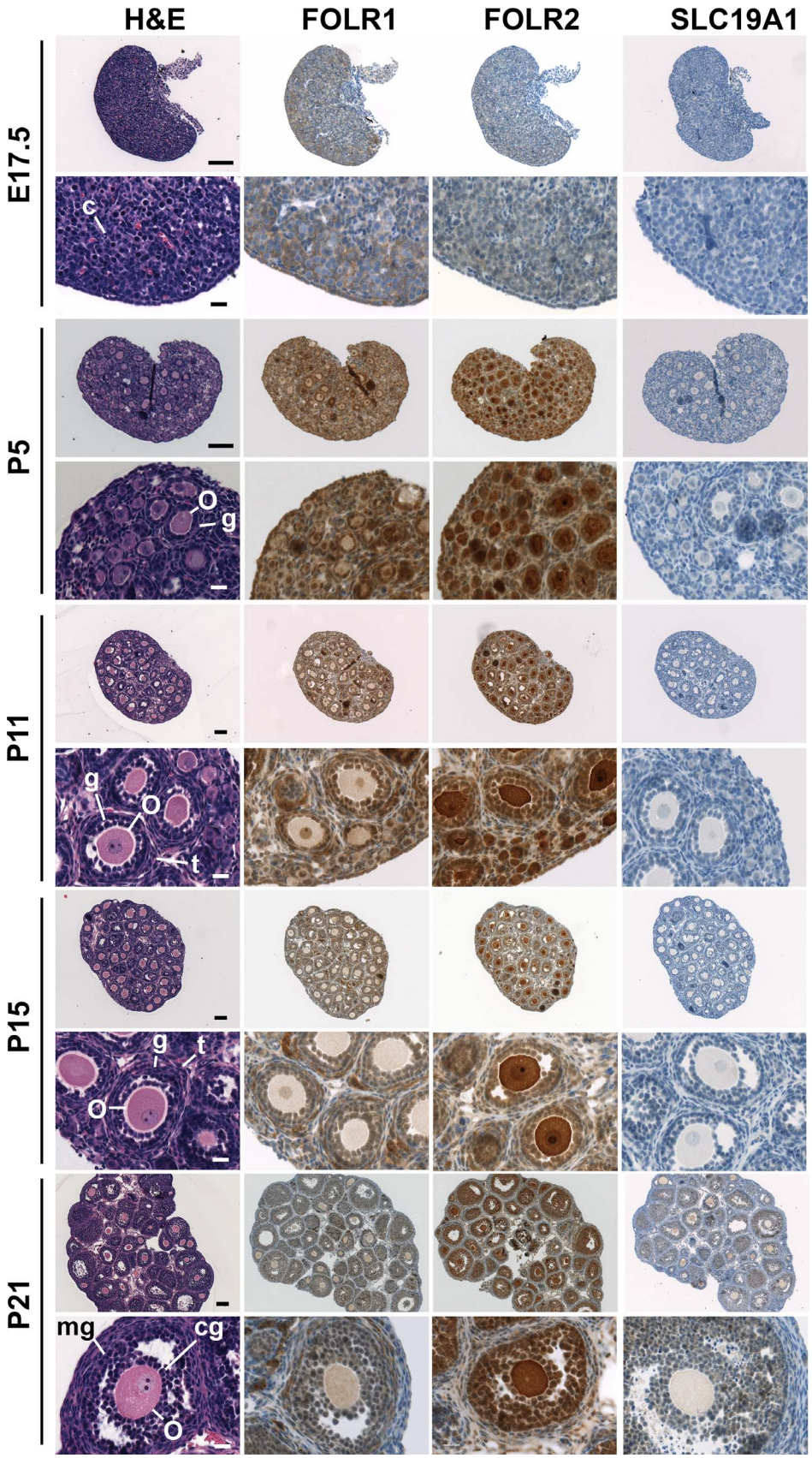


FIG. 1. Immunohistochemical detection of folate transporter proteins in neonatal ovaries. Immunohistochemistry was performed on ovary sections from E17.5 fetal ovaries and neonatal ovaries on P5, P11, P15, and P21, as indicated at the left of the rows. Sections are stained with hematoxylin/eosin (H&E), or immunohistochemistry was performed with antibodies against FOLR1, FOLR2, or SLC19A1 (RFC1 transporter), as indicated at the top for each column. For each embryonic or fetal stage, the images in the upper rows were obtained with a 10× objective with scale bars shown at the lower right of the images in the H&E column indicating 100 μm (images for E17.5 and P5 are shown at 2-fold higher magnification than P11–21 to facilitate visualization). The lower rows for each stage were obtained using a 63× objective with the scale bars indicating 20 μm (images for all stages are shown at the same magnification). E17.5 ovaries consist primarily of germline cysts (c) that contain meiotic oocytes at the pachytene/diplotene border, while each stage of neonatal ovary contains a cohort of growing

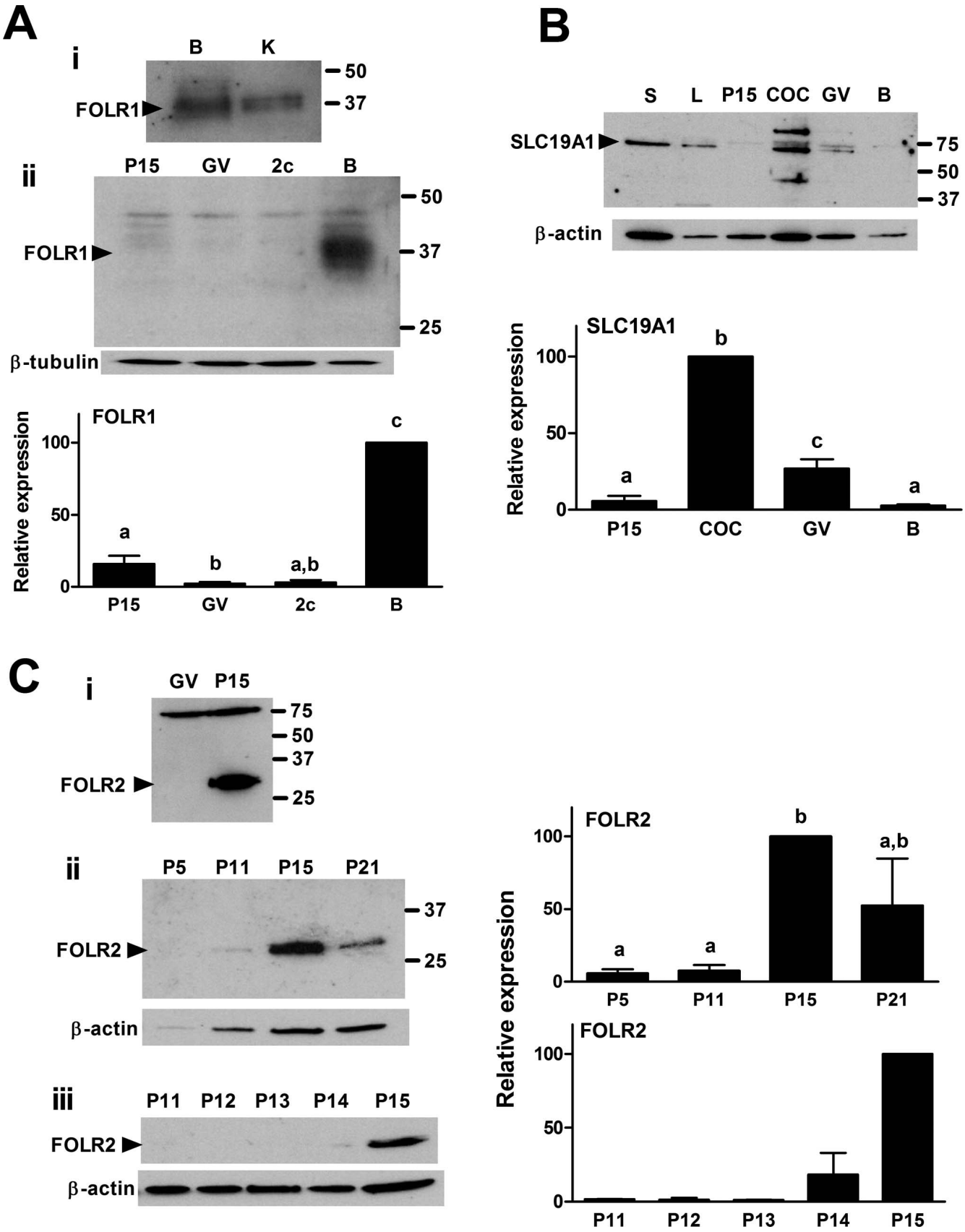


FIG. 2. Western blot detection of folate transporter proteins. **A**) FOLR1. **i**) A band was detected for blastocysts (35 in lane) whose size extended mainly above the expected size of unglycosylated FOLR1 (32 kDa). The diffuse, extended band is similar to that previously reported for human FOLR1, where this

oocytes and follicles at a characteristic stage of development [38–40]. Developing follicles (P5–21) consist of growing oocytes (O) stained pink and surrounding granulosa cells (g) stained darker purple. Theca cells (t) are clearly discernable surrounding the granulosa layers from P11. On P21, antral follicles have developed consisting of fully grown oocytes surrounded by cumulus granulosa cells (cg) and mural granulosa cells (mg). At each stage, the ovarian surface epithelium forms a single-cell layer at the outer surface of the ovary. Images manipulations were limited to resizing. Examples shown are typical of three independent repeats.

expression pattern is consistent with our previous finding that RFC1 activity is high in cumulus cells but absent in oocytes and preimplantation embryos [25].

Substantial FOLR2 immunoreactivity, in contrast, appeared to be present in growing oocytes, but not in fully grown GV oocytes from adult ovaries (Fig. 2C). When different stages of growing oocytes were compared, FOLR2 protein was detected at high levels in P15 oocytes, with little or no FOLR2 present at earlier stages (Fig. 2C).

We attempted to confirm that the band present on Western blots with P15 oocytes was FOLR2 by comparing it to mouse placenta, a tissue reported to express FOLR2 [41]. However, we found that the band in placenta ran at a lower apparent size (~27 kDa) than the band (~30 kDa) in oocytes (Fig. 3). Although there have been few studies of FOLR2 expression, it has been reported that human FOLR2 exists in several forms that differ in their level of glycosylation [41, 42]. Thus, we sought to determine whether the discrepant band size between oocytes and placenta was due to differential glycosylation by treating the samples with peptide-N-glycosidase F prior to gel electrophoresis. However, although overexpressed human FOLR2 shifted to a lower apparent size after deglycosylation in a pattern identical to previous reports [41, 42], the bands present in mouse placenta did not shift while those in P15 oocytes decreased only slightly and did not decrease to the size observed in placenta (Fig. 3). Thus, the different apparent sizes of the protein putatively identified as FOLR2 in placenta and oocytes remains unexplained.

Finally, we investigated the expression and localization of folate transporters in P15 oocytes, COCs, and blastocysts by immunofluorescence. Consistent with the preceding results and our previous functional studies [25], FOLR1 immunofluorescence was present in blastocysts but not P15 oocytes, while a low level of immunofluorescence signal appeared in cumulus granulosa cells but not the enclosed GV oocyte (Fig. 4A), consistent with FOLR1 immunoreactivity in cumulus granulosa cells in P21 ovaries by immunocytochemistry (Fig. 1). FOLR2 immunofluorescence, in contrast, was present near the plasma membranes of P15 oocytes but not in COCs or blastocysts (Fig. 4B). The FOLR2 antibody also labeled nucleoli in oocytes and blastocysts, which was presumably nonspecific. A similar reaction within nuclei of oocytes was seen with immunohistochemistry (Fig. 1). SLC19A1 (RFC1) immunofluorescence was significant only in cumulus cells (Fig. 4C), consistent with our previous functional studies [25] and immunoreactivity with granulosa cells in P21 antral follicles detected by immunohistochemistry (Fig. 1).

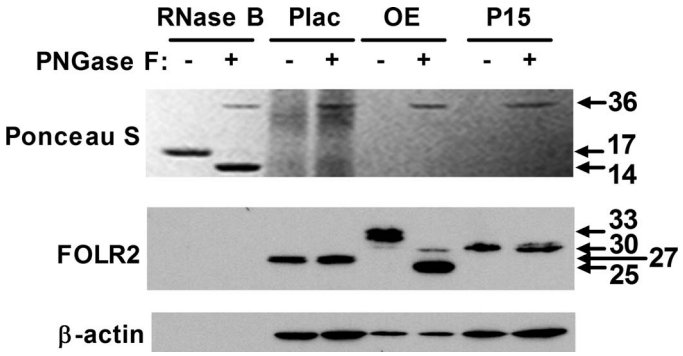


FIG. 3. Deglycosylation of FOLR2. PNGase F treatment (500 U per reaction) was used to determine whether N-glycosylation affected the apparent size of FOLR2 detected in mouse placenta and P15 growing oocytes. Numbers at right indicate calculated molecular weights. The activity of PNGase F was confirmed using RNAse B detected with Ponceau S staining (top), showing the expected decrease in apparent size from 17 to 14 kDa. The added PNGase F was visible as a band at 36 kDa. Western blot analysis of the same membrane for FOLR2 (middle) did not detect any shift in the FOLR2 band (27 kDa) in mouse placenta lysate (10 μg/lane). Overexpressed human FOLR2 (200 ng), however, was decreased from 33 to 25 kDa upon deglycosylation. P15 oocyte (50 oocytes per lane) FOLR2 appeared to undergo a small decrease from about 31 to 30 kDa upon treatment with PNGase F. The β-actin served as a loading control (bottom). The example shown is representative of four independent repeats.

FOLR2 immunofluorescence located mainly near the plasma membrane of P15 oocytes would be consistent with the expected localization of a receptor at the cell surface that is endocytosed and recycled to the cell surface. To investigate this immunofluorescence localization and whether it changes during oocyte growth, we quantified fluorescence intensity across oocytes at several developmental stages (Fig. 5, A and B). This confirmed a preferential FOLR2 immunofluorescence localization near the oocyte membrane at all stages assessed except P5 oocytes, with P15 oocytes exhibiting the highest membrane-to-cytoplasmic intensity ratio (Fig. 5C).

### *Folate Transport Activity in Growing Oocytes*

To measure folate transport, we used the model folate LV, also known as folinic acid, that we had previously extensively validated with preimplantation embryos [25]. We measured [$^3$H] LV transport into oocytes at different stages of their growth from small growing oocytes (~30 μm) to fully grown

was due to glycosylation [48]. A doublet near the same size was present in positive control kidney lysate (0.5 μg). Blastocysts were used because previous functional data implied that FOLR1 is active in blastocysts [25]. **ii**) Western blots with growing oocytes from neonatal ovaries (P15), fully grown oocytes (GV) from adult ovaries, 2-cell embryos (2c), and blastocysts (B) were probed for FOLR1 expression. Each lane was loaded with 50 oocytes or embryos except 200 P15 oocytes were loaded; β-tubulin served as a loading control. The example shown is representative of three repeats whose band densities are quantified in the graph, normalized to the average density for blastocysts (set arbitrarily to 100). Numbers at right indicate positions of size markers (in all panels). **B**) SLC19A1 (RFC1). Western blots with growing oocytes (P15), cumulus-oocyte complexes (COCs), and fully grown oocytes (GV) from adult ovaries and blastocysts (B) were probed for SLC19A1 expression. COCs were included as a positive control because previous functional data implied that FOLR1 is active in COCs but not blastocysts [25]. Spleen (S) and liver (L) lysates (5 μg each) were included as positive control tissues. Each lane contained 50 oocytes, COCs, or embryos. A doublet of bands near the expected size of SLC19A1 (62 kDa) was clearly evident in COCs with faint bands in GV oocytes. Additional bands were present in COCs, which could represent dimers and fragments or nonspecific bands; β-actin served as a loading control. The example shown is representative of three repeats, with mean relative densities graphed as in **A**. **C**) FOLR2. **i**) Western blots were probed for FOLR2 in growing oocytes (P15) and fully grown (GV) oocytes (100 per lane), which indicated expression in growing oocytes but little in fully grown oocytes (representative example of two repeats) as evidenced by a band near the expected size of FOLR2 (30 kDa). **ii**) Growing oocytes from P5, P11, P15, and P21 neonates were compared (50 per lane), showing the greatest immunoreactivity in P15 oocytes (representative example of three repeats). **iii**) Comparing growing oocytes each day from P11 to P15 (50 per lane) showed that the band increased on P15 (representative example of two repeats); β-actin served as a loading control. Relative mean densities are graphed as in **A** (right). Bars labeled with different letters are significantly different ($P < 0.05$, ANOVA with Tukey multiple comparison test, except in **Ciii**, where two repeats were done and thus no statistical analysis carried out). Quantifications and statistical tests are provided to aid in visualizing expression patterns, primarily to differentiate clear expression from low/absent expression. It should be noted that they are based on equal numbers of embryos or oocytes per lane and thus cannot be normalized to total protein or a protein with constant expression across stages.

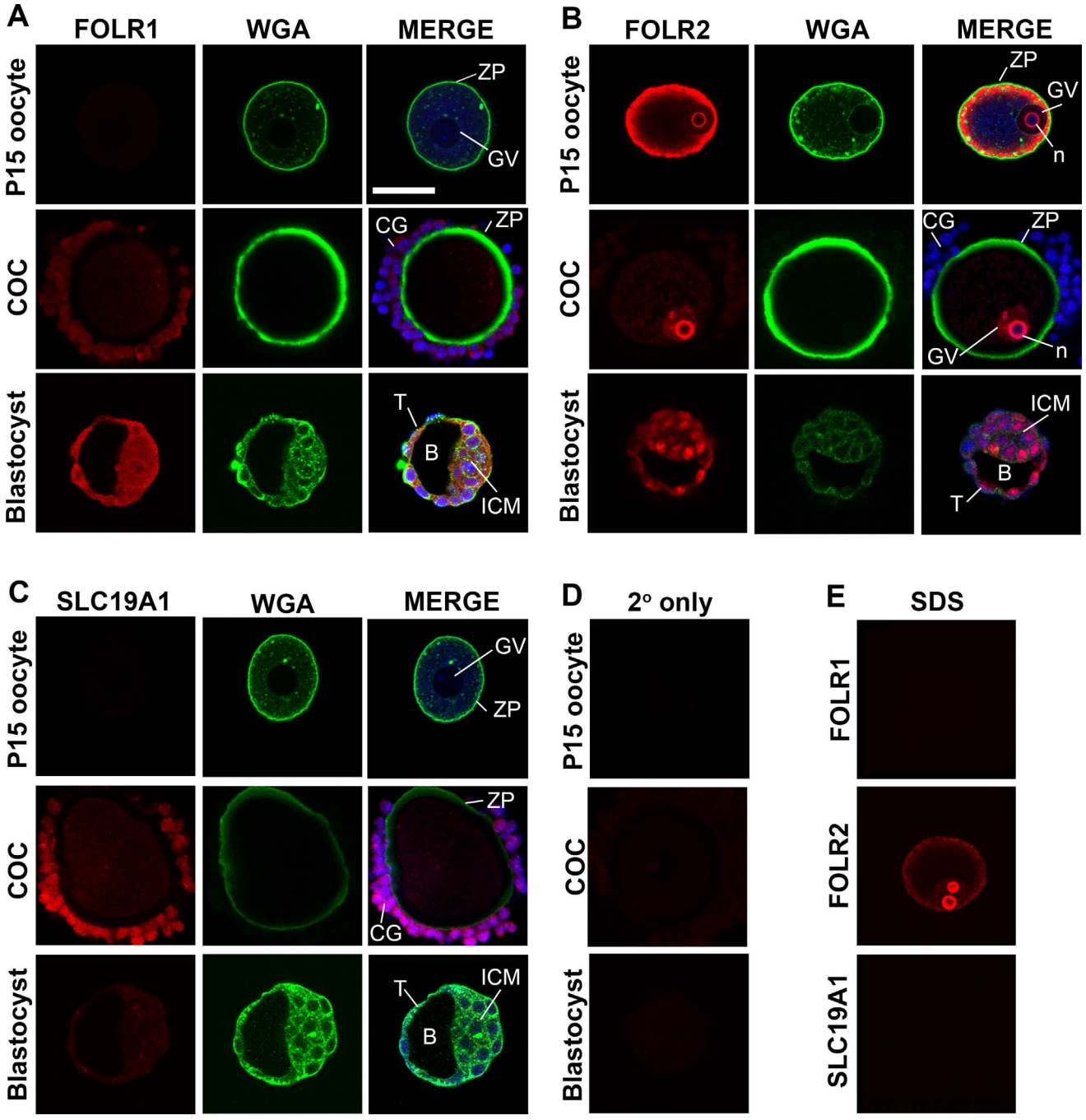


FIG. 4. Immunofluorescence detection of folate transporter proteins. Immunofluorescence detection for FOLR1 (**A**), FOLR2 (**B**), and SLC19A1 (**C**) was performed for growing (P15) oocytes, COCs from adult female mice, and blastocysts as indicated for each row at the left. Structures that are labeled in the merged images at the left of **A**–**C** are the zona pellucida (ZP), germinal vesicle (nucleus, GV), cumulus granulosa cells (CG), trophectoderm (T), inner cell mass (ICM), blastocoel cavity (B), and nucleoli (n). The scale bar shown in the top right image in **A** indicates 50 μm and applies to all images. Immunofluorescence (red) is shown in the first column of each panel with the antibody indicated at the top in **A**–**D**. Wheat germ agglutinin (Alexa-488 WGA, green) strongly binds to the zona pellucida remnants on the surface of P15 oocytes and the zona pellucida in COCs and weakly to the blastocyst surfaces, and was used for visualization in the middle columns. Merged images are shown at the left of **A**–**C**, combining the antibody image (red), WGA (green), and DNA visualized with Hoechst 33342 (blue). For the FOLR2 antibody (**B**), there was apparent nonspecific binding to nuclei and particularly nucleioli in addition to cytoplasmic/membrane staining, which was also seen in immunohistochemistry (Fig. 1). Secondary (2°) antibody alone only produced minimal fluorescence (**D**). Because detection of FOLR2 immunofluorescence required epitope unmasking (1% SDS, 2.5 min) after fixation, we confirmed that neither FOLR1 nor SLC19A1 immunofluorescence (antibodies indicated at left) was present in P15 oocytes after this treatment (**E**). This also provided a control showing that the apparent FOLR2 immunofluorescence in P15 oocytes is not likely the result of nonspecific IgG binding because the same concentrations of rabbit IgG were present for FOLR1 and SLC19A1 as for FOLR2. The minimum and maximum brightness levels were set so 0 represents the lowest values in the images, and the maximum was set above the brightest, to maximize dynamic range. In the merged images, each channel was set separately to optimize visualization. The same settings were used for each image shown, except that the brightness was set higher for WGA in blastocysts than P15 oocytes or COCs because fluorescence was dimmer. The images shown are representative of fluorescence patterns observed in three independent repeats, each of which contained 5–10 oocytes or embryos, except for (**E**), where there were two independent repeats.

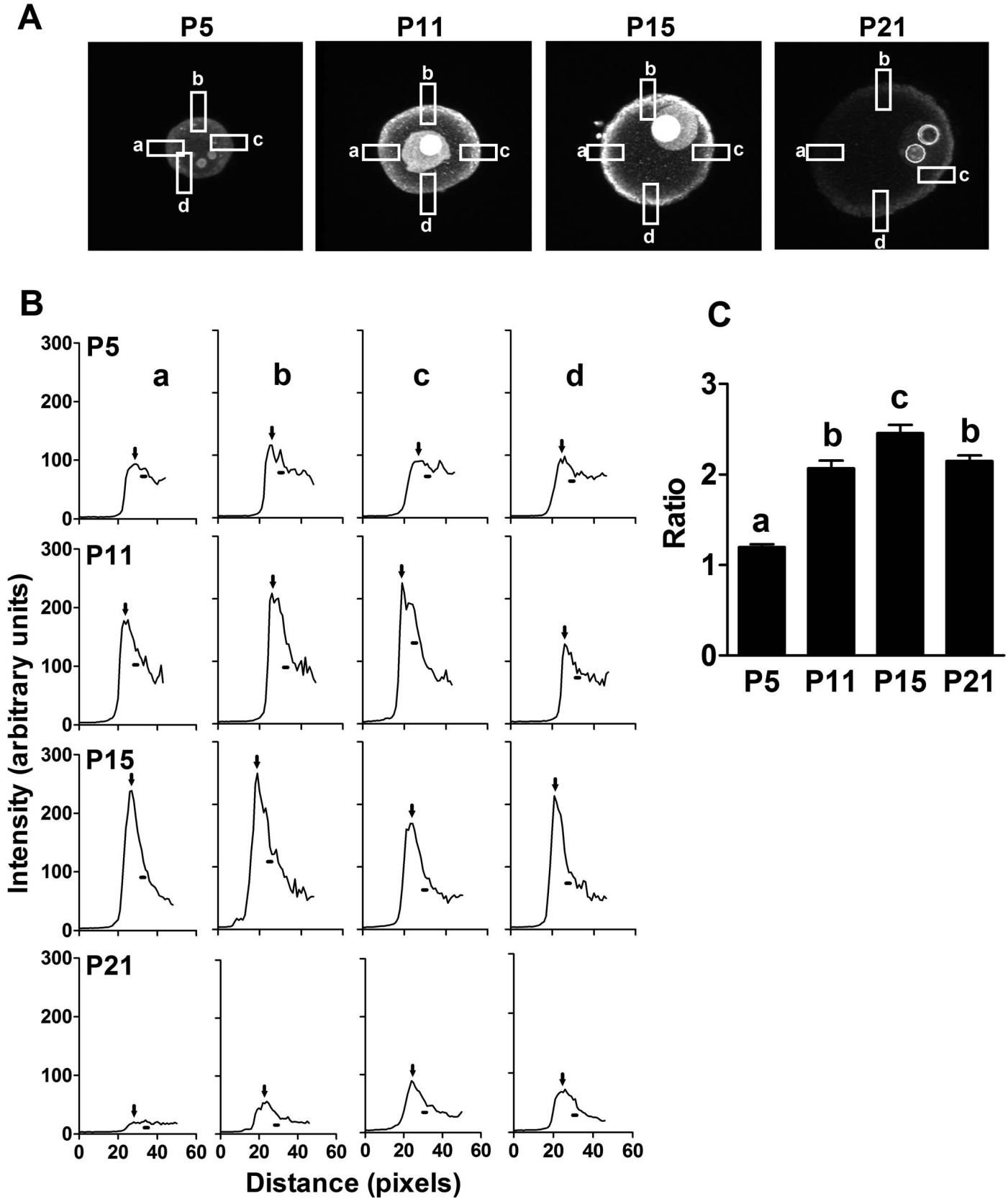


FIG. 5. Localization of FOLR2 immunofluorescence in growing oocytes. **A**) FOLR2 immunofluorescence intensity was quantified as a function of distance in four orthogonal locations across the membranes of P5, P11, P15, and P21 growing oocytes. The typical regions of interest in which fluorescence was measured are indicated by rectangles (a–d) in the examples shown. Images were not adjusted. **B**) Fluorescence intensities were plotted as a function of radial distance for the regions specified in **A**. The arrows in the examples shown indicate the location where intensity at the oocyte membrane was obtained and the short line segments the positions where cytoplasmic measurements were calculated as the average within the range indicated by the segment (10 pixels). **C**) Plasma membrane-to-cytoplasm fluorescence ratios were plotted as shown in the examples in **A** and **B** for a total of 17–25 oocytes measured at each stage (distributed among $n = 3$ independent repeats). Bars that do not share the same letter are significantly different by ANOVA with Tukey post hoc test.

oocytes (~75 μm) that were obtained from neonatal ovaries and divided by diameter into 5 μm bins. Unexpectedly, we detected LV transport activity above background in oocytes only within a single size bin, 65–69 μm (Fig. 6A).

To confirm this result, we isolated oocytes from adult ovaries after stimulation of follicular development with eCG. A similar pattern was obtained, with a substantial level of LV transport activity measured in oocytes of diameters only in the range of 70–74 μm (Fig. 6B). Again, little transport activity was detectable in small oocytes or in fully grown oocytes.

Finally, we determined whether intact follicles exhibited the same unexpected peak of folate transport that was found in isolated growing oocytes. Because P15 neonatal ovaries contain the highest proportion of growing oocytes in the 65–69 μm range, we compared follicles isolated from P15 ovaries to those at P5, P11, and P21. Only follicles derived from P15 ovaries exhibited LV transport activity (Fig. 6C), which is consistent with the results obtained with isolated oocytes.

### *Characteristics of Folate Transport Activity in Oocytes*

Folate transport via folate receptors can be functionally distinguished from that by RFC1. A clear difference is the mode of transport because folate receptors require endocytosis while RFC1 functions as an anion antiporter [23]. Thus, the two mechanisms can be clearly differentiated by their inhibition by the stilbene SITS [25, 36], which is a broad-spectrum inhibitor of anion transport, or inhibition by dynasore [25, 37], which is a small molecule inhibitor of dynamin that blocks endocytosis. We previously validated the use of these inhibitors in preimplantation embryos and COCs [25]. Here, we assessed the effects of SITS and dynasore on LV transport in P15 growing oocytes. Excess unlabeled LV inhibited [$^3$H] LV transport by >80%, confirming that a large fraction of the measured transport in P15 oocytes was by a saturable transporter (Fig. 7A). SITS had no effect on LV transport, indicating that RFC1 was unlikely to mediate detectable levels of folate transport in P15 growing oocytes. In contrast, dynasore reduced LV transport to the level of nonspecific transport (Fig. 7B), indicating that a folate receptor was likely responsible for LV transport. Because of the similar transport characteristics of FOLR1 and FOLR2, it was not possible to further differentiate the transporter involved by transport measurements.

We had previously shown that cumulus granulosa cells surrounding fully grown GV stage oocytes take up folates via RFC1, but that no detectable folates were transferred to the enclosed oocyte [25]. Our immunohistochemistry results (Fig. 1) indicated that FOLR1 and FOLR2 may each be expressed in granulosa cells on P15 and RFC1 (SLC19A1) is present at least by P21. Thus, it is possible that granulosa cells in growing follicles could take up folates by one or more of these mechanisms and transfer them to the enclosed oocyte. Thus, we examined whether the surrounding follicular cells might have a role in folate transport into P15 growing oocytes, where folate transport into follicles was detected. Intact follicles were incubated with [$^3$H] LV, and the rate of transport of [$^3$H] LV was then measured into intact follicles or into oocytes removed after the incubation (designated A = after) and also compared to oocytes that had been removed from follicles before incubation with [$^3$H] LV (designated B = before). Isolated oocytes (B) exhibited the highest level of LV transport, while oocytes that had been inside follicles during incubation (A) accumulated comparatively little LV (Fig. 8). This confirms that folate transport occurs principally in the oocyte, while

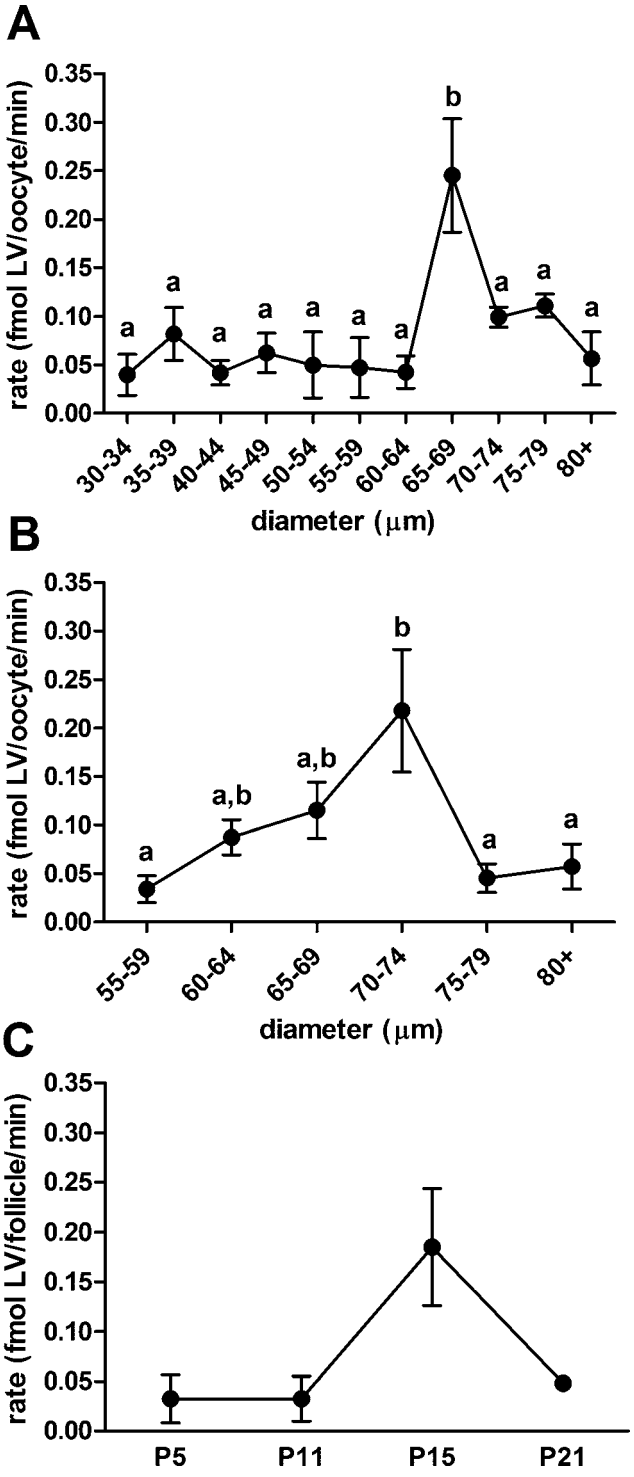


FIG. 6. [$^3$H] LV transport by growing oocytes. **A**) Growing oocytes obtained from neonatal (P5–21) ovaries were sorted by diameter into 5 μm wide bins and incubated with 2 μM [$^3$H] LV for 20 min in KSOM medium (total transport) or with 1 mM unlabeled LV added (nonsaturable transport). The difference between the total and nonsaturable components was graphed. Each point represents the mean ± SEM of three independent repeats. Points that do not share letters are significantly different (ANOVA, Tukey post hoc test). **B**) LV transport was measured as in **A** in growing oocytes obtained from adult ovaries (three independent repeats). Points that do not share letters are significantly different (ANOVA, Tukey post hoc test). **C**) LV transport was measured in intact follicles isolated from P5, P11, P15, and P21 neonatal ovaries as in **A** (three independent repeats). A significant difference was reported by ANOVA ($P = 0.03$), however the variability in measurements at P15 prevented detection of significant differences between specific groups by Tukey post hoc test.

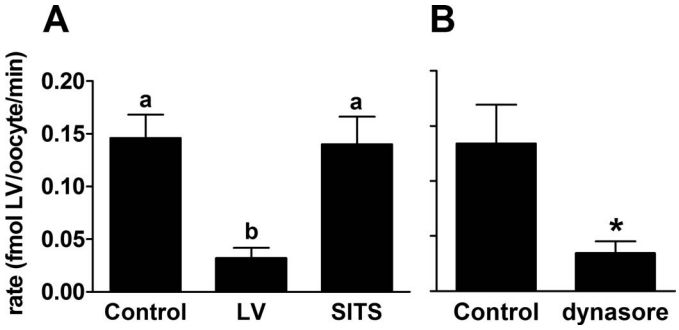


FIG. 7. Characteristics of LV transport in P15 growing oocytes. P15 oocytes were incubated with 2 μM [$^3$H] LV for 20 min in KSOM to obtain LV transport rates. **A**) The rate of transport was determined in P15 oocytes under control conditions (no addition), with 1 mM unlabeled LV added, or in the presence of the anion transport inhibitor SITS (1 mM). Bars that do not share the same letter are significantly different ($P < 0.01$, ANOVA, Tukey post hoc test). Approximately 80% of LV transport was saturable, as revealed by competition with excess unlabeled LV. SITS had no significant effect on transport. **B**) The rate of transport was assessed in the presence of dynasore (80 μM) and in control conditions (0.1% dimethyl sulfoxide). Oocytes were pretreated with dynasore or vehicle for 30 min before transport was measured in the continued presence of dynasore or vehicle. The means with and without dynasore were significantly different (*$P = 0.02$; paired Student *t*-test). In both **A** and **B**, bars represent the mean ± SEM of five repeats.

transfer of folates taken up by the follicle to the enclosed oocyte appears to play a minor, if any, role.

## DISCUSSION

The results we report here indicate immunodetection of the folate transport proteins RFC1 (SLC19A1), FOLR1, and FOLR2 in various cell types within the developing mouse ovary. However, only FOLR2 appeared to be detected in growing oocytes, as indicated by immunohistochemistry, Western blots, and whole-mount immunofluorescence. The lack of detection of substantial FOLR1 or SLC19A1 (RFC1) in oocytes likely reflects low or absent expression of those proteins because FOLR1 was found to be clearly present in blastocysts and SLC19A1 in cumulus cells using both immunofluorescence and Western blots, as predicted from previous measurements of folate transport characteristics [25].

Our data are consistent with a folate receptor mediating the folate transport activity that appears in growing oocytes. Folate transport measurements indicated that transport into oocytes was completely inhibited by blocking endocytosis with dynasore but was insensitive to inhibition of anion exchange by SITS, implicating a folate receptor rather than RFC1. Although it is not possible to clearly differentiate the two murine folate receptor homologues based on transport characteristics, expression of FOLR2 protein in oocytes appeared to be detected by three different techniques, each of which failed to find substantial FOLR1, making FOLR2 a more likely candidate. Furthermore, quantification of membrane localization showed that FOLR2 immunofluorescence was most highly localized near the plasma membrane in P15 oocytes, coincident with the stage where folate transport activity was detected.

A question that remains to be answered, however, is why the putative FOLR2 bands in oocytes and placenta differed because the known alternate transcripts arising from the murine *Folr2* gene reportedly produce the same FOLR2 protein (NP_001290160) and we did not detect N-glycosylation in the mouse proteins (unlike in overexpressed human FOLR2).

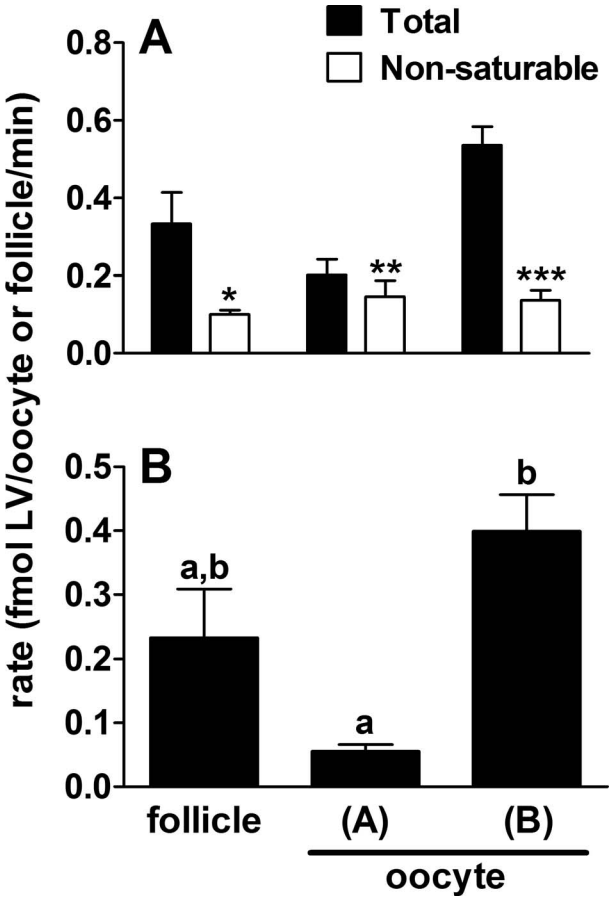


FIG. 8. Effect of follicular granulosa cells on transport of LV into P15 growing oocytes. **A**) The rate of transport of [$^3$H] LV was measured for intact P15 follicles containing an oocyte (follicle), oocytes that were removed from follicles after incubation with [$^3$H] LV (oocyte [A]), or oocytes removed from follicles before incubation with [$^3$H] LV (oocyte [B]), as indicated at bottom for both panels. The total rate of LV transport and the nonsaturable component of LV transport in the presence of 1 mM unlabeled LV were determined. In each case, there was a significant component of saturable transport (*$P = 0.02$, **$P = 0.006$, ***$P < 0.0001$ by *t*-tests), although the difference for oocytes that had been inside follicles during incubation (oocyte [A]) was small. **B**) The nonspecific rates were subtracted from the total rates (data in **A**) to yield the saturable components of LV transport for each preparation. Oocytes that were removed from follicles before they were incubated with [$^3$H] LV as isolated oocytes (oocyte [B]) took up LV at a much higher rate than oocytes that were removed from follicles after the intact follicle had been incubated with [$^3$H] LV (oocyte [A]). Bars that do not share letters are significantly different ($P < 0.01$ by ANOVA, Tukey post hoc test). Five independent repeats were performed.

The size differences could potentially represent unreported alternative transcripts or posttranslational modifications, but this remains to be investigated. We also cannot rule out that the transport in growing oocytes is due to FOLR1 that we were not able to clearly detect.

The most unexpected finding was that, despite the apparent presence of folate transport proteins in oocytes and in the coupled granulosa cells throughout oogenesis, folate transport activity only appeared during an extremely narrow window of oocyte growth. We detected folate transport activity only in neonatal growing oocytes 65–69 μm in diameter and high folate transport activity in oocytes 70–74 μm in diameter from adult ovaries. Both of these correspond to oocytes at approximately 85%–90% of final size because the diameter of fully grown neonatal oocytes is ~10% less than those from

the adult cycling ovary [43]. In both cases, folate transport activity disappeared when the oocytes were fully grown.

There is little known about folate requirements in mammalian oocytes. One study of in vitro follicle culture starting with P13–14 follicles investigated the effect of reducing methyl donors in culture medium on follicle growth and oocyte developmental potential [44]. They found that eliminating added folates from the medium in conjunction with the absence of several other components of the folate and methionine cycles severely reduced follicle growth and oocyte competence to proceed through meiotic maturation. However, the effect of omitting folates alone was not determined.

The folate cycle of 1C metabolism is crucial for nucleic acid synthesis and for synthesis of SAM. Oocytes do not replicate DNA and are transcriptionally silent when fully grown, but repression of transcription only starts at P17 in neonatal oocytes and is not entirely completed until they are fully grown, with similar developmental timing in oocytes from cycling adult females [45, 46]. Thus, an active folate cycle may be required for the completion of maternal transcript synthesis to supply the egg with stored maternal mRNA.

Alternatively, there may be a heightened requirement for SAM synthesis toward the end of oocyte growth. Following the nearly complete erasure of DNA methylation in primordial germ cells, an oocyte-specific methylome is established during oocyte growth, with methylation occurring as oocytes grow from 50 μm diameter (around P10) to fully grown [15, 47]. Thus, much of the de novo DNA methylation in oocytes may occur on P15 and later, and activation of the folate cycle may be needed to accumulate an increased pool of SAM for establishing the oocyte methylome.

Finally, the transport of folate into oocytes may reflect a need to accumulate and store folates for use during preimplantation embryogenesis. Folate transport activity does not develop in the embryo until later in preimplantation development, and no folate transport is detected in oocytes during meiotic maturation or in mature eggs [25]. Furthermore, an endogenous pool of folate is present in fertilized eggs that is sufficient to sustain all of preimplantation development in vitro in the absence of folate in the culture medium [11, 12]. Therefore, folates accumulated at the end of oocyte growth may be stored to be used during early embryogenesis.

In summary, growing mouse oocytes exhibit a transient burst of folate transport activity as they near full growth, which is inactive in fully grown oocytes. The characteristics of folate transport in oocytes are consistent with folate receptor-mediated endocytosis, possibly by the FOLR2 isoform. Further work is needed to determine the function of the accumulated folates in oocytes or embryos.

## REFERENCES


1. Fox JT, Stover PJ. Folate-mediated one-carbon metabolism. In: Gerald L (ed.), Vitamins & Hormones, Folic Acid and Folates, vol. 79. London: Academic Press; 2008:1–44.
2. Tibbetts AS, Appling DR. Compartmentalization of mammalian folate-mediated one-carbon metabolism. Ann Rev Nutr 2010; 30:57–81.
3. Loenen WA. S-adenosylmethionine: jack of all trades and master of everything? Biochem Soc Trans 2006; 34:330–333.
4. Stover PJ. Physiology of folate and vitamin B12 in health and disease. Nutr Rev 2004; 62:S3–S12.
5. Fowler B. The folate cycle and disease in humans. Kidney Int Suppl 2001; 78:S221–S229.
6. Lu SC. S-Adenosylmethionine. Int J Biochem Cell Biol 2000; 32: 391–395.
7. Katz JE, Dlakic M, Clarke S. Automated identification of putative methyltransferases from genomic open reading frames. Mol Cell Proteomics 2003; 2:525–540.
8. Copp AJ, Stanier P, Greene ND. Neural tube defects: recent advances, unsolved questions, and controversies. Lancet Neurol 2013; 12:799–810.
9. Ikeda S, Koyama H, Sugimoto M, Kume S. Roles of one-carbon metabolism in preimplantation period–effects on short-term development and long-term programming. J Reprod Dev 2012; 58:38–43.
10. Pelland AM, Corbett HE, Baltz JM. Amino acid transport mechanisms in mouse oocytes during growth and meiotic maturation. Biol Reprod 2009; 81:1041–1054.
11. O'Neill C. Endogenous folic acid is essential for normal development of preimplantation embryos. Hum Reprod 1998; 13:1312–1316.
12. Kwong WY, Adamiak SJ, Gwynn A, Singh R, Sinclair KD. Endogenous folates and single-carbon metabolism in the ovarian follicle, oocyte and pre-implantation embryo. J Reprod Fertil 2010; 139:705–715.
13. Zhang B, Denomme MM, White CR, Leung KY, Lee MB, Greene ND, Mann MR, Trasler JM, Baltz JM. Both the folate cycle and betaine-homocysteine methyltransferase contribute methyl groups for DNA methylation in mouse blastocysts. FASEB J 2015; 29:1069–1079.
14. Smith ZD, Meissner A. DNA methylation: roles in mammalian development. Nat Rev Genet 2013; 14:204–220.
15. Lucifero D, Mann MRW, Bartolomei MS, Trasler JM. Gene-specific timing and epigenetic memory in oocyte imprinting. Hum Mol Genet 2004; 13:839–849.
16. Hiura H, Obata Y, Komiyama J, Shirai M, Kono T. Oocyte growth-dependent progression of maternal imprinting in mice. Genes Cells 2006; 11:353–361.
17. Reik W, Dean W, Walter J. Epigenetic reprogramming in mammalian development. Science 2001; 293:1089–1093.
18. Smith ZD, Chan MM, Mikkelsen TS, Gu H, Gnirke A, Regev A, Meissner A. A unique regulatory phase of DNA methylation in the early mammalian embryo. Nature 2012; 484:339–344.
19. Lee MB, Kooistra M, Zhang B, Slow S, Fortier AL, Garrow TA, Lever M, Trasler JM, Baltz JM. Betaine homocysteine methyltransferase is active in the mouse blastocyst and promotes inner cell mass development. J Biol Chem 2012; 287:33094–33103.
20. Qiu A, Jansen M, Sakaris A, Min SH, Chattopadhyay S, Tsai E, Sandoval C, Zhao R, Akabas MH, Goldman ID. Identification of an intestinal folate transporter and the molecular basis for hereditary folate malabsorption. Cell 2006; 127:917–928.
21. Dixon KH, Lanpher BC, Chiu J, Kelley K, Cowan KH. A novel cDNA restores reduced folate carrier activity and methotrexate sensitivity to transport deficient cells. J Biol Chem 1994; 269:17–20.
22. Ganapathy V, Smith SB, Prasad PD. SLC19: the folate/thiamine transporter family. Pflugers Arch 2004; 447:641–646.
23. Zhao R, Matherly LH, Goldman ID. Membrane transporters and folate homeostasis: intestinal absorption and transport into systemic compartments and tissues. Expert Rev Mol Med 2009; 11:e4.
24. Antony AC. Folate receptors. Ann Rev Nutr 1996; 16:501–521.
25. Kooistra M, Trasler JM, Baltz JM. Folate transport in mouse cumulus-oocyte complexes and preimplantation embryos. Biol Reprod 2013; 89:63.
26. Zhao R, Diop-Bove N, Visentin M, Goldman ID. Mechanisms of membrane transport of folates into cells and across epithelia. Ann Rev Nutr 2011; 31:177–201.
27. Kamen BA, Wang MT, Streckfuss AJ, Peryea X, Anderson RG. Delivery of folates to the cytoplasm of MA104 cells is mediated by a surface membrane receptor that recycles. J Biol Chem 1988; 263:13602–13609.
28. Brzezinska A, Winska P, Balinska M. Cellular aspects of folate and antifolate membrane transport. Acta Biochim Pol 2000; 47:735–749.
29. Lawitts JA, Biggers JD. Culture of preimplantation embryos. Methods Enzymol 1993; 225:153–164.
30. Erdogan S, FitzHarris G, Tartia AP, Baltz JM. Mechanisms regulating intracellular pH are activated during growth of the mouse oocyte coincident with acquisition of meiotic competence. Dev Biol 2005; 286: 352–360.
31. Sorensen RA, Wassarman PM. Relationship between growth and meiotic maturation of the mouse oocyte. Dev Biol 1976; 50:531–536.
32. Zhou C, Baltz JM. JAK2 mediates the acute response to decreased cell volume in mouse preimplantation embryos by activating NHE1. J Cell Physiol 2013; 228:428–438.
33. Baltz JM, Corbett HE, Richard S. Measuring transport and accumulation of radiolabeled substrates in oocytes and embryos. Methods Mol Biol 2013; 957:163–178.
34. Van Winkle LJ. Transport kinetics. In: Van Winkle LJ (ed.), Biomembrane Transport. San Diego: Academic Press; 1999:65–131.
35. Van Winkle LJ, Campione AL, Farrington BH. Development of system B0,+ and a broad-scope Na(+)-dependent transporter of zwitterionic amino acids in preimplantation mouse conceptuses. Biochim Biophys Acta 1990; 1025:225–233.

36. Sierra EE, Brigle KE, Spinella MJ, Goldman ID. Comparison of transport properties of the reduced folate carrier and folate receptor in murine L1210 leukemia cells. Biochem Pharmacol 1995; 50:1287–1294.
37. Kirchhausen T, Macia E, Pelish HE. Use of dynasore, the small molecule inhibitor of dynamin, in the regulation of endocytosis. In: Balch C, William E (ed.), Methods in Enzymology: Small GTPAses in Disease, Part A, vol. 438. London: Academic Press; 2008:77–93.
38. Peters H. The development of the mouse ovary from birth to maturity. Acta Endocrinol (Copenh) 1969; 62:98–116.
39. Pepling ME. From primordial germ cell to primordial follicle: mammalian female germ cell development. Genesis 2006; 44:622–632.
40. Findlay JK, Hutt KJ, Hickey M, Anderson RA. How is the number of primordial follicles in the ovarian reserve established? Biol Reprod 2015; 93:111.
41. Ratnam M, Marquardt H, Duhring JL, Freisheim JH. Homologous membrane folate binding proteins in human placenta: cloning and sequence of a cDNA. Biochemistry 1989; 28:8249–8254.
42. Shen F, Wang H, Zheng X, Ratnam M. Expression levels of functional folate receptors alpha and beta are related to the number of N-glycosylated sites. Biochem J 1997; 327(Pt 3):759–764.
43. Wassarman PM, Schultz RM, Letourneau GE, LaMarca MJ, Josefowicz WJ, Bleil JD. Meiotic maturation of mouse oocytes in vitro. Adv Exp Med Biol 1979; 112:251–268.
44. Anckaert E, Romero S, Adriaenssens T, Smitz J. Effects of low methyl donor levels in culture medium during mouse follicle culture on oocyte imprinting establishment. Biol Reprod 2010; 83:377–386.
45. Bouniol-Baly C, Hamraoui L, Guibert J, Beaujean N, Szollosi MS, Debey P. Differential transcriptional activity associated with chromatin configuration in fully grown mouse germinal vesicle oocytes. Biol Reprod 1999; 60:580–587.
46. De La Fuente R, Eppig JJ. Transcriptional activity of the mouse oocyte genome: companion granulosa cells modulate transcription and chromatin remodeling. Dev Biol 2001; 229:224–236.
47. Tomizawa S, Nowacka-Woszuk J, Kelsey G. DNA methylation establishment during oocyte growth: mechanisms and significance. Int J Dev Biol 2012; 56:867–875.
48. Roberts SJ, Petropavlovskaja M, Chung KN, Knight CB, Elwood PC. Role of individual N-linked glycosylation sites in the function and intracellular transport of the human alpha folate receptor. Arch Biochem Biophys 1998; 351:227–235.